

Majorana noise model and its influence on the power spectrum

Shumeng Chen(陈书梦), Sifan Ding(丁思凡), Zhen-Tao Zhang(张振涛), and Dong E. Liu(刘东)
Citation: Chin. Phys. B, 2024, 33 (**1**): 017101. DOI: 10.1088/1674-1056/acfd19
Journal homepage: http://cpb.iphy.ac.cn; http://iopscience.iop.org/cpb

What follows is a list of articles you may be interested in

Switching plasticity in compensated ferrimagnetic multilayers for neuromorphic computing

Weihao Li(李伟浩), Xiukai Lan(兰修凯), Xionghua Liu(刘雄华), Enze Zhang(张恩泽), Yongcheng Deng(邓永城), and Kaiyou Wang(王开友)
Chin. Phys. B, 2022, 31 (**11**): 117106. DOI: 10.1088/1674-1056/ac89dd

Electronic structures of vacancies in $Co_3Sn_2S_2$

Yuxiang Gao(高于翔), Xin Jin(金鑫), Yixuan Gao(高艺璇), Yu-Yang Zhang(张余洋), and Shixuan Du(杜世萱)
Chin. Phys. B, 2021, 30 (**7**): 077102. DOI: 10.1088/1674-1056/abfa05

Non-Hermitian Kitaev chain with complex periodic and quasiperiodic potentials

Xiang-Ping Jiang(蒋相平), Yi Qiao(乔艺), and Junpeng Cao(曹俊鹏)
Chin. Phys. B, 2021, 30 (**7**): 077101. DOI: 10.1088/1674-1056/abfa08

Explicit forms of zero modes in symmetric interacting Kitaev chain without and with dimerization

Yiming Wang(王一鸣), Zhidan Li(李志聃), Qiang Han(韩强)
Chin. Phys. B, 2018, 27 (**6**): 067101. DOI: 10.1088/1674-1056/27/6/067101

Topological phase boundary in a generalized Kitaev model

Da-Ping Liu(刘大平)
Chin. Phys. B, 2016, 25 (**5**): 057101. DOI: 10.1088/1674-1056/25/5/057101

Majorana noise model and its influence on the power spectrum

Shumeng Chen(陈书梦)[1], Sifan Ding(丁思凡)[1], Zhen-Tao Zhang(张振涛)[2], and Dong E. Liu(刘东)[1,3,4,5,†]

[1] *State Key Laboratory of Low Dimensional Quantum Physics, Department of Physics, Tsinghua University, Beijing* 100084, *China*
[2] *School of Physics Science and Information Technology, Shandong Key Laboratory of Optical Communication Science and Technology, Liaocheng University, Liaocheng* 252059, *China*
[3] *Beijing Academy of Quantum Information Sciences, Beijing* 100193, *China*
[4] *Frontier Science Center for Quantum Information, Beijing* 100084, *China*
[5] *Hefei National Laboratory, Hefei* 230088, *China*

(Received 21 July 2023; revised manuscript received 9 September 2023; accepted manuscript online 26 September 2023)

Majorana quantum computation offers a potential approach to securely manipulating and storing quantum data in a topological manner that may effectively resist the decoherence induced by local noise. However, actual Majorana qubit setups are susceptible to noise. In this study, from a quantum dynamics perspective, we develop a noise model for Majorana qubits that accounts for quasi-particle poisoning and Majorana overlapping with fluctuation. Furthermore, we focus on Majorana parity readout methodologies, specifically those leveraging an ancillary quantum dot, and carry out an in-depth exploration of continuous measurement techniques founded on the quantum jump model of a quantum point contact. Utilizing these methodologies, we proceed to analyze the influence of noise on the afore-mentioned noise model, employing numerical computation to evaluate the power spectrum and frequency curve. In the culmination of our study, we put forward a strategy to benchmark the presence and detailed properties of noise in Majorana qubits.

Keywords: Majorana zero mode, topological quantum computation, topological devices, decoherence and noise in qubits

PACS: 71.10.Pm, 74.20.Mn, 03.65.Yz, 03.67.Lx **DOI:** 10.1088/1674-1056/acfd19

1. Introduction

Non-Abelian anyons offer a novel methodology for potentially achieving fault-tolerant quantum computation, wherein quantum information is encoded using non-local degrees of freedom and quantum operations are manipulated in a manner that is topologically protected.[1–8] Of particular interest in this context are the Majorana zero modes that can be potentially hosted by topological superconductors, which are widely regarded as the most realizable candidates for topological quantum computation.[9–24]

Numerous theoretical proposals have been put forward regarding the readout and manipulation of Majorana qubits in superconducting nanowires.[23,25–42] In these designs, the qubit is encoded in a non-local manner using the parity of pairs of Majorana zero modes. In topological quantum computing, the readout of Majorana parity is of significant importance, and a number of methods have been proposed for this purpose. These include projective measurement schemes[28,29] and continuous measurement approaches with the use of quantum dot ancillaries,[26,43] as well as a conductance-based readout method in a dot-free configuration under a tunable magnetic flux.[30] A recent publication[44] briefly discusses the above different techniques used for Majorana parity readout. Among these methods, the use of quantum dot ancillaries for measurement displays considerable promise due to its scalability.[29] In work by Steiner *et al.*,[43] a continuous measurement scheme employing quantum dot ancillaries is suggested to distinguish between Majorana parities. Specifically, the power spectrum of current correlation is utilized under the diffusion limit of a quantum point contact to achieve this objective. Building upon this idea, we examine the physical parameter discussed in Wiseman and Milburn's work[45] and derive the power spectrum of current in the quantum point contact utilizing the quantum jump model. Based on this model, we then study a readout method for Majorana parities. It is suggested that Majorana readout based on the quantum jump model may be more practical for real materials and experimental devices.

While Majorana qubits possess certain theoretical advantages, quantum information can still be affected by both internal and external noise sources.[46–53] Therefore, refining the noise model and evaluating its impact is crucial for the progress of Majorana quantum computation. The Majorana noise model was initially developed to study the impact of noise on quantum channels by Knapp and coworkers[53] In this regard, the model was used to investigate the pseudo-threshold of the Majorana qubit realization of Bacon–Shor code. To further investigate the effect of noise from a quantum dynamics perspective, we proposed a concise Majorana noise model based on the master equation in Lindblad form. We combined this model with the Majorana noise model and conducted numerical research to examine the influence of noise on the readout signal. Our study yielded insights into how dif-

†Corresponding author. E-mail: dongeliu@mail.tsinghua.edu.cn
© 2024 Chinese Physical Society and IOP Publishing Ltd

ferent types and intensities of noise affect the power spectrum and frequency curve. Based on these findings, we developed an approach for detecting noise in the Majorana qubit. We employed a quaternion array $\left(\Gamma_1, \Gamma_2, \varepsilon_{\rm hyb}, g^2\right)$ to classify the noise, while peak width, peak weight, fusion point and curve structure were used to label the frequency curve as it varied with quasi-particle poisoning rate. By analyzing the characteristics of the frequency curve, we obtained crucial information about the noise, thus introducing an approach for investigating noise in the Majorana qubit.

The present paper is structured as follows. Section 2 provides the formulation of the noise model for quasi-particle poisoning and Majorana overlapping noise based on the master equation in Lindblad form. In Section 3, we offer a comprehensive review of the Majorana parity readout technique and develop it further through the use of the quantum jump model for quantum point conduction coupled with an ancillary quantum dot. Subsequently, in Section 4, we evaluate the impact of noise on the readout signal through numerical calculations using the model presented in Section 2 and the methodology elaborated in Section 3; based on these results, we propose an approach for detecting noise in the Majorana qubit.

2. Majorana noise model

The issue of noise in Majorana qubits has been extensively discussed in previous works such as Refs. [29,46,47,50,51,53,54]. As a complement to these discussions, this section presents a mathematical formulation in Lindblad form to model the effects of quasi-particle poisoning noise and Majorana overlapping with fluctuations.

2.1. Single quasi-particle poisoning event

Quasi-particle poisoning represents a major source of noise in Majorana qubits.

This phenomenon is primarily attributed to the presence of superfluous electrons within the device, as well as the ensnarement of those single electrons by the Majorana wave function. The creation of those single electrons is generally provoked by thermal excitation or radiation-induced excitement of Cooper pairs within the superconducting material.[47,53] Because quasi-particle poisoning can directly change the parity state of a Majorana qubit, it can lead to either qubit error or leakage, causing the Majorana qubit to deviate from its original computational subspace, resulting in negative impacts on the storage and retrieval of information for topological quantum bits.

In this section, we adopt the quantum trajectory approach outlined in Refs. [55,56] to construct our noise model. Our starting point is the simplest noise event, namely, a Majorana quasi-particle poisoning event, denoted as $\hat{\gamma}_1$, that occurs in one of the Majorana zero modes. We assume that the quasi-particle poisoning rate, denoted as Γ_1, remains constant and is entirely determined by the environment, i.e., independent of the system state. At time t, the quasi-particle poisoning event $\mathrm{d}N(t) = 1$ occurs with a probability of $p_1 = \Gamma_1 \mathrm{d}t$ during the time interval $\mathrm{d}t$. Here, $N(t)$ represents the number of quasi-particle poisoning events up to time t. The operator associated with this event can be expressed as

$$\hat{A}_1 = \sqrt{\Gamma_1 \mathrm{d}t}\hat{\gamma}_1, \tag{1}$$

such that

$$p_1 = \mathrm{Tr}[\hat{A}_1 \rho \hat{A}_1] = \Gamma_1 \mathrm{d}t. \tag{2}$$

Then, by the conservation of probability, we can define the operator when no event happens $\hat{A}_0$ by

$$\hat{A}_1^\dagger \hat{A}_1 + \hat{A}_0^\dagger \hat{A}_0 = \hat{I}, \tag{3}$$

then

$$\hat{A}_0 = \hat{I} - \Gamma_1 \frac{\hat{I}}{2}\mathrm{d}t. \tag{4}$$

Thus, we can get the state for both evolutions. For $\mathrm{d}N(t) = 1$,

$$|\Psi(t+\mathrm{d}t)\rangle = \hat{\gamma}_1 |\Psi(t)\rangle. \tag{5}$$

For $\mathrm{d}N(t) = 0$,

$$|\Psi(t+\mathrm{d}t)\rangle = |\Psi(t)\rangle. \tag{6}$$

Then, the stochastic Schrödinger equation is

$$\mathrm{d}|\Psi(t)\rangle = (\hat{\gamma}_1 - \hat{I})\mathrm{d}N(t)|\Psi(t)\rangle. \tag{7}$$

Then by Ito rules and taking average $E[\mathrm{d}N] = \Gamma_1 \mathrm{d}t$, we can get the master equation of quasi-particle poisoning

$$\dot{\rho}_{\rm M} = \Gamma_1(\hat{\gamma}_1 \rho_{\rm M} \hat{\gamma}_1 - \rho_{\rm M}), \tag{8}$$

where $\rho_{\rm M}$ present the density matrix of the Majorana qubit. The noise model can also be obtained when a quasi-particle poisoning event affects the whole Majorana zero mode in the same way,

$$\dot{\rho}_{\rm M} = \sum_i \Gamma_i(\hat{\gamma}_i \rho_{\rm M} \hat{\gamma}_i - \rho_{\rm M}). \tag{9}$$

In order to obtain an estimate of the quasi-particle rate Γ_i, we can make use of the values reported in Refs. [47,51]. These values take into account all potential sources of uncorrelated quasi-particle poisoning events that contribute to Γ_i.

2.2. Overlapping with fluctuation

Taking into account the finite size of nanowires, the effective Hamiltonian for the Majorana system takes the form[9,37]

$$\hat{H}_{\rm M} = \mathrm{i}\varepsilon_{\rm hyb}\hat{\gamma}_1\hat{\gamma}_2. \tag{10}$$

Here, the value of $\varepsilon_{\rm hyb}$ was discussed in Refs. [9,37,54]. However, we assume that the hybridization energy may exhibit fluctuations, leading to a corresponding fluctuating Hamiltonian given by

$$\hat{H}_{\rm MF} = {\rm i}\left(\varepsilon_{\rm hyb} + g\xi(t)\right)\hat{\gamma}_1\hat{\gamma}_2. \tag{11}$$

In this expression, the term $g\xi(t)$ represents the fluctuation contribution and we assume that it follows Gaussian statistics such that

$$g\xi(t){\rm d}t = g{\rm d}W(t). \tag{12}$$

Here, g represents the intensity of the noise and ${\rm d}W$ denotes the Wiener increment. Using these assumptions, we can obtain the following property for $\delta\varepsilon(t)$:

For Gaussian white noise,

$$\langle (g\xi(t))g\xi(\tau)\rangle = g^2\delta(t-\tau), \tag{13}$$

where $\delta(t-\tau)$ is the Dirac function. Then

$$\left\langle \left(\int_0^t (\delta\varepsilon(t))^2 \right\rangle = g^2 t. \right. \tag{14}$$

With certain encoding, we can have ${\rm i}\gamma_1\gamma_2 = \sigma_z$ under a qubit basis. Then, by Ito rules, we can get the propagator

$${\rm e}^{-{\rm i}\hat{H}_{\rm MF}{\rm d}t} = \hat{I} - {\rm i}\varepsilon_{\rm hyb}{\rm d}t\hat{\sigma}_z - {\rm i}g{\rm d}W\hat{\sigma}_z - \frac{g^2}{2}{\rm d}t\hat{I}. \tag{15}$$

Then, by taking the average of stochastic wave function increment ${\rm d}\rho = {\rm d}(|\psi\rangle\langle\psi|)$, we can get the master equation for the fluctuating hybridization energy.

$$\dot{\rho}_{\rm M} = -{\rm i}\varepsilon_{\rm hyb}[\hat{\sigma}_z, \rho_{\rm M}] + g^2(\hat{\sigma}_z\rho_{\rm M}\hat{\sigma}_z - \rho_{\rm M}). \tag{16}$$

So far, we have obtained the master equation for Majorana overlapping with Gaussian fluctuation.

3. Majorana parity readout by continuous measurement

Several proposals for Majorana readout methods utilizing quantum dot ancillaries have been presented in the literature.[26,28,29,57] In contrast, Steiner *et al.*[43] introduced a novel technique that relies on continuous measurement. This method utilizes the power spectrum of current correlation in a quantum point contact, in conjunction with a quantum dot, to differentiate between different Majorana parities. A recent review article[44] provides a succinct overview of various Majorana readout approaches. We begin by introducing the effective tunneling Hamiltonian for a Majorana coupled with quantum dots[30]

$$\hat{H}_{\rm tunn} = {\rm e}^{-{\rm i}\frac{\hat{\phi}}{2}}(t_1\hat{\gamma}_1 + t_2\hat{\gamma}_2)\hat{c}_1^\dagger + {\rm H.c.} \tag{17}$$

The operator ${\rm e}^{\pm{\rm i}\frac{\hat{\phi}}{2}}$ increases/decreases the charge number of the superconductor by one charge number unit and $\hat{\phi}$ is the phase operator of the superconductor; $\hat{c}_1$ and $\hat{c}_1^\dagger$ are the annihilation and creation operator of a quantum dot in a few-electron occupancy regime. $\hat{\gamma}_1$, $\hat{\gamma}_2$ are the Majorana operators, which can change the parity of the electron number in the superconductor. t_1 and t_2 are the corresponding tunneling amplitudes between the quantum dot and $\hat{\gamma}_1$ and $\hat{\gamma}_2$.

In order to have a better understanding of the system, two different methods are proposed in the literature. The first method, as discussed in Ref. [57], employs the basis $|n,p\rangle$ where $|1,p\rangle = {\rm e}^{-{\rm i}\frac{\hat{\phi}}{2}}c_1^\dagger\gamma_1|0,p\rangle$. Here, $n = 0,1$ and $p = \pm 1$ denote the eigenvalues of the quantum dot occupation and combined parity $p = p_{12}(-1)^n$, respectively, where $p_{12} = {\rm i}\gamma_1\gamma_2$ represents the Majorana parity. Alternatively, the second method described in Ref. [30] involves replacing ${\rm e}^{\pm{\rm i}\frac{\hat{\phi}}{2}}$ with the spin operator $\hat{s}_\pm$, and considering the only two relevant states $|n_0\rangle$ and $|n_0+1\rangle$ associated with the tunneling process, where n_0 denotes the electron number of the superconductor before the tunneling event. In this approach, the Majorana and spin operators are combined into a fermion operator: $\hat{f}$: $\hat{\gamma}_1\hat{s}_+ \to \hat{f}^\dagger$, $\hat{\gamma}_1\hat{s}_- \to \hat{f}$, $\hat{\gamma}_2\hat{s}_+ \to {\rm i}(-1)^{n_0}\hat{f}^\dagger$, $\hat{\gamma}_2\hat{s}_- \to {\rm i}(-1)^{n_0+1}\hat{f}$. By employing the above approach, we can derive the matrix representation of the tunneling Hamiltonian within the stated basis

$$\hat{H}_{\rm tunn} = \begin{pmatrix} 0 & t_1^* + {\rm i}pt_2^* \\ t_1 - {\rm i}pt_2 & 0 \end{pmatrix}. \tag{18}$$

The Majorana parity-dependent effective tunneling amplitude, denoted by t_p, is given by $t_p = t_1 - {\rm i}pt_2$. Alternatively, we can express t_p in terms of the phase difference between t_1 and t_2 as $t_p = |t_1|(1 - {\rm i}\,{\rm e}^{{\rm i}\theta}p\lambda)$, where $\lambda = |t_2|/|t_1|$ and $\theta = {\rm Arg}(t_2/t_1)$. This expression serves as the fundamental premise for all Majorana parity readout techniques that employ quantum dot ancillaries.

The article[29] discusses three methods for measuring the parity-dependent tunneling amplitude in a Majorana system. The first method involves energy-level spectroscopy, whereby the ground-state energy difference is measured. The second and third methods rely on the measurement of the differential capacitance and the average dot occupation number, respectively.

Reference [28] proposes a Majorana readout method based on the direct measurement of the parity-dependent Rabi-oscillation frequency, which originates from the parity-dependent tunneling amplitude. However, this method requires a fast projective measurement of the quantum dot, which poses experimental challenges. Therefore, Ref. [43] suggests a continuous measuring approach to overcome these challenges. In this approach, the Rabi-oscillation frequency is obtained by measuring the current correlation in a quantum point contact coupled to the quantum dot ancillary. The

setup for continuous measuring is shown in Fig. 1. As discussed in Refs. [45,55,58–61], two models describe the current in a quantum point contact. In addition, Ref. [43] employs the diffusive model. Here, by considering the discussion in Refs. [45,62], we explore the quantum jump model as a suitable framework for simulating scenarios that involve a photon number detector.

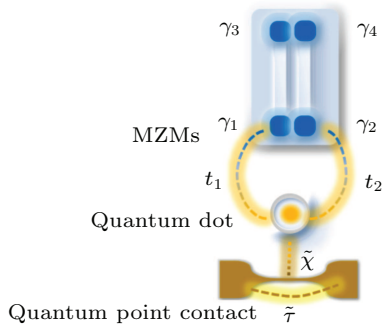


Fig. 1. Setup for continuous measurement of Majorana parity.

Subsequently, the following Hamiltonian for the perfect Majorana island connected to a quantum dot is introduced:

$$\hat{H}_{\mathrm{MQD}} = \hat{H}_{\mathrm{QD}} + \hat{H}_{\mathrm{tunn}}. \tag{19}$$

In the low-temperature regime and under the strong magnetic field required for a topological phase,[11,20] the effective Hamiltonian for a single spinless fermion level can be approximated for the quantum dot

$$\hat{H}_{\mathrm{QD}} = \varepsilon_1 \hat{n}_1, \tag{20}$$

where ε_1 is the dot level and $\hat{n}_1 = \hat{c}_1^{\dagger}\hat{c}_1$ is the particle number operator for the electron of the quantum dot. In the work by Karzig *et al.*,[29] the charging energy terms of the quantum dot and the superconducting island are taken into consideration. By employing the parameter transformation method discussed in Ref. [57], the mutual charging energy term and the dot level term are effectively combined into a single charging energy term, which can be expressed as $\hat{H}_{\mathrm{C+QD}} = \varepsilon_{\mathrm{C}}(\hat{n}_1 - n_{1\mathrm{g}})^2$, where $\hat{n}_1$ represents the particle number operator of the quantum dot and $n_{1\mathrm{g}}$ is the quantum dot's ground state occupation number. The parameter ε_{C} denotes the effective dimensionless gate voltage of the superconductor–quantum dot system and the effective charging energy. The detailed treatment can be found in the appendix of Ref. [57]. As the system operates in the resonance regime, where the energy of the quantum dot is approximately equal to the charging energy of the superconductor, for simplicity, the authors use ε_1 as the effective tuning parameter and express the effective Hamiltonian of the quantum dot as $\varepsilon_1\hat{n}_1$. This simplification does not affect the matrix form or the measurement result.

Subsequently, the quantum point contact is integrated as a dot occupation number monitor in the subsequent stage, enabling the extraction of parity information from the current flowing through the quantum point contact. We follow a strategy similar to that used for a double quantum dot[60,61,63,64] and obtain the dynamics for the Majorana–quantum dot setup

$$\dot{\rho}(t) = -\mathrm{i}\left[\hat{H}_{\mathrm{MQD}}, \rho(t)\right] + \hat{\mathcal{D}}\left[\tilde{\tau} + \tilde{\chi}\hat{n}_1\right]\rho(t), \tag{21}$$

where $\rho(t)$ is the density matrix for the quantum dot and Majoranas coupled with the quantum dot. $\hat{n}_1 = \hat{c}_1^{\dagger}\hat{c}_1$ is the particle number operator for quantum dot, $\tilde{\tau}$ and $\tilde{\chi}$ are defined as $D = |\tilde{\tau}|^2 = 2\pi e|T_{00}|^2 g_{\mathrm{L}} g_{\mathrm{R}} V/$ and $D' = |\tilde{\tau} + \tilde{\chi}|^2 = 2\pi e|T_{00} + \chi_{00}|^2 g_{\mathrm{L}} g_{\mathrm{R}} V/$, T_{00} and X_{00} are tunneling amplitudes near the average chemical potential, g_{L} and g_{R} are the densities of states for the left and right reservoirs, V is the external bias applied across the quantum point contact; thus D and D' represent the average tunneling rates through the quantum point contact without and with one electron in dot 1. $\hat{\mathcal{D}}$ is defined as

$$\hat{\mathcal{D}}[\hat{B}]\rho = \hat{B}\rho\hat{B}^{\dagger} - \left(\hat{B}^{\dagger}\hat{B}\rho + \rho\hat{B}^{\dagger}\hat{B}\right)/2. \tag{22}$$

The Hamiltonian for the quantum point contact can be expressed as follows:

$$\begin{aligned}\hat{H}_{\mathrm{QPC}} = &\sum_k \left(\omega_k^{\mathrm{L}}\hat{c}_{\mathrm{L}k}^{\dagger}\hat{c}_{\mathrm{L}k} + \omega_k^{\mathrm{R}}\hat{c}_{\mathrm{R}k}^{\dagger}\hat{c}_{\mathrm{R}k}\right) \\ &+ \sum_{k,q}\left(T_{kq}\hat{c}_{\mathrm{L}k}^{\dagger}\hat{c}_{\mathrm{R}q} + T_{qk}^{*}\hat{c}_{\mathrm{R}q}^{\dagger}\hat{c}_{\mathrm{L}k}\right),\end{aligned} \tag{23}$$

where $\hat{c}_{\mathrm{L}k}$, $\hat{c}_{\mathrm{R}k}$ and ω_k^{L}, ω_k^{R} are, respectively, the electron annihilation operators and the energy levels for the left and right reservoir states at wave number k. T_{kq} is the tunneling amplitude for the corresponding tunneling channel. The Hamiltonian describing the interaction between the quantum dot and quantum point contact is given as

$$\hat{H}_{\mathrm{coup}} = \sum_{k,q}\hat{c}^{\dagger}\hat{c}\left(\chi_{kq}\hat{a}_{\mathrm{L}k}^{\dagger}\hat{a}_{\mathrm{R}q} + \chi_{qk}^{*}\hat{a}_{\mathrm{R}q}^{\dagger}\hat{a}_{\mathrm{L}k}\right). \tag{24}$$

When the quantum dot is occupied, the effective tunneling amplitude of quantum point contact changes from $T_{kq} \to T_{kq} + \chi_{kq}$. Next, we follow the approach presented in Refs. [55,63] and obtain the conditional current in the quantum point contact based on the quantum jump model

$$\langle I\rangle_{\mathrm{c}}(t) = eD + e\left(D' - D\right)\langle\hat{n}_1\rangle_{\mathrm{c}}(t). \tag{25}$$

The two values currently depend on the dot occupation number. The reduced two-time-correlation function is defined as

$$R(\tau) = \mathbb{E}[I(t+\tau)I(t)] - \mathbb{E}[I(t+\tau)]\mathbb{E}[I(t)], \tag{26}$$

where $\mathbb{E}[\,]$ present the ensemble average.

In the general case, it is preferable to conduct numerical investigations on $R(\tau)$. However, in the case where $\varepsilon_1 = 0$, an analytical expression is available, the current correlation for Majorana coupled to the quantum dot is

$$R_p(\tau) = eI_{\infty}\delta(\tau) + \frac{(\delta I)^2}{4}\left(\frac{\mu_{p+}\mathrm{e}^{\mu_{p-}\tau} - \mu_{p-}\mathrm{e}^{\mu_{p+}\tau}}{\mu_{p+} - \mu_{p-}}\right), \tag{27}$$

where $\mu_{p\pm} = -(\kappa/4) \pm \sqrt{(\kappa/4)^2 - (2|t_p|)^2}$, $I_\infty = e(D'+D)/2$ is the steady-state current, $\delta I = e(D-D')$ is the difference between the two average currents and $\kappa = |\tilde{\chi}|^2$. The corresponding power spectrum is defined as

$$S(\omega) = \int_{-\infty}^{\infty} \mathrm{d}\tau R_p(\tau) \mathrm{e}^{-\mathrm{i}\omega\tau}. \tag{28}$$

Then

$$S_p(\omega) = S_0 + \frac{(\delta I)^2}{4} \frac{|t_p|^2 \kappa}{\left(\omega^2 - (2|t_p|)^2\right)^2 + (\kappa/2)^2 \omega^2}, \tag{29}$$

where $S_0 = e^2(D'+D)$ represents the shot noise. Thus we can distinguish between different Majorana parities by the power spectrum of the current in quantum point contact. Figure 2 shows the numerical simulation of the power spectrum for different Majorana parity values.

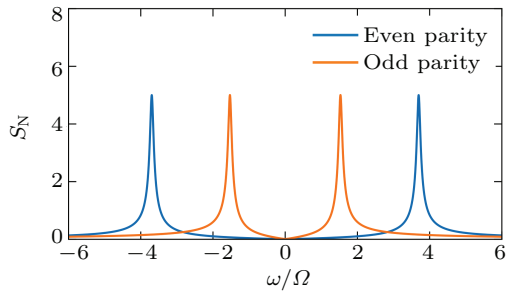


Fig. 2. Power spectrum for different Majorana parity values. The normalized power spectrum, as defined here, is represented by $S_N = \frac{S(\omega)-S_0}{I_\infty \delta I}$, where the parameters are specified as follows: $\lambda = 1$, $\theta = \pi/4$, $\kappa = 0.2|t_1|$, and $|t_1| = \Omega$. It is worth noting that Ω serves as the reference frequency unit here.

4. Noise influence on parity readout

The scheme presented in Ref. [43] posits a power spectrum current correlation technique for ideal Majorana qubits, featuring zero noise, as a means of Majorana parity readout. In this scenario, the current correlation can be computed from the fixed parity subspace, much akin to the double quantum dot system with a constant tunneling amplitude $t_1 + \mathrm{i}pt_2$. This approach remains valid for other parity readout methods for Majorana qubits, such as measuring the average occupation number of the quantum dot, for which only the subspace warrants consideration. Nevertheless, when probing the impact of Majorana noise, comprehensive consideration of the full Hilbert space, inclusive of both the Majorana qubit and the quantum dot, becomes indispensable.

For quasi-particle poisoning, we can get the dynamics of a Majorana coupled with a quantum dot

$$\dot{\rho} = -\mathrm{i}[\hat{H}_{\mathrm{MQD}}, \rho] + \mathcal{D}[\tau + \chi\hat{n}_1]\rho + \sum_{i=1,2} \Gamma_i(\hat{\gamma}_i \rho \hat{\gamma}_i - \rho). \tag{30}$$

For Majorana overlapping, we can get

$$\dot{\rho} = -\mathrm{i}[\hat{H}_{\mathrm{MQD}}, \rho] - \mathrm{i}[\hat{H}_{\mathrm{M}}, \rho] + \mathcal{D}[\tau + \chi\hat{n}_1]\rho. \tag{31}$$

For Majorana overlapping with fluctuation, we can get

$$\dot{\rho} = -\mathrm{i}[\hat{H}_{\mathrm{MQD}}, \rho] - \mathrm{i}[\hat{H}_{\mathrm{M}}, \rho] + \mathcal{D}[\tau + \chi\hat{n}_1]\rho + g^2(\hat{\sigma}_z \rho \hat{\sigma}_z - \rho). \tag{32}$$

As the analytical solution to the aforementioned master equation is considerably intricate, our discussion primarily focuses on the numerical outcomes.

4.1. Quasi-particle poisoning

For quasi-particle poisoning, the following special scenarios are first considered: when $\Gamma_1 = \Gamma_2$, when $\Gamma_1 \neq 0$ and $\Gamma_2 = 0$, and when $\Gamma_1 = 0$ and $\Gamma_2 \neq 0$. The first situation describes a homogeneous environment, whereas the second and third cases represent specific instances of an inhomogeneous noise environment. This study chiefly examines three parameter regions concerning the quasi-particle rate: (1) when the quasi-particle poisoning rate is significantly smaller than the Rabi oscillation frequency, (2) when the quasi-particle poisoning rate is of the same order of magnitude as the Rabi oscillation frequency, and (3) when the quasi-particle poisoning rate is much greater than the Rabi oscillation frequency.

In the context of homogeneous quasi-particle poisoning noise, we can denote the noise intensity by $\Gamma = \Gamma_1 = \Gamma_2$. As demonstrated in Fig. 3(a), when the quasi-particle poisoning rate is very small ($\Gamma \ll |t_1|$), the peak frequency exhibits an insignificant shift. This indicates that the parity measurement result can be obtained with high precision under such a noise intensity. As the quasi-particle poisoning rate increases, the two peaks move towards each other, accompanied by an increase in peak width, and eventually merge into a single peak at the Rabi oscillation frequency ($\Gamma \approx |t_1|$). This implies that, in this range, the two peaks cannot be distinguished and the Majorana parity cannot be obtained from the measurement. As the quasi-particle rate further increases, the merged peak shifts its frequency to zero. This implies that when the quasi-particle poisoning rate is much larger than the Rabi oscillation frequency, the current in QPC is described by shot noise, which is similar to the behavior observed in coupled quantum dots when $\kappa \gg 4\Omega$. Here, $\kappa = |\tilde{\chi}|^2$ represents the coupling strength between the quantum dot and QPC, and Ω represents the coupling strength between quantum dots. In this case, the electron will be localized in the quantum dot, a phenomenon also referred to as the quantum Zeno effect. Figures 3(b)–3(d) illustrate the power spectrum at different levels of noise intensity.

Subsequently, an observation was made that the power spectrum's structure changes in the presence of quasi-particle poisoning. As depicted in Figs. 4(a) and 4(b), a secondary peak emerges at the location of the opposite parity with a comparatively smaller weight for each parity. Here, weight corresponds to the area enclosed by the corresponding peak. The secondary peak remains negligible under a relatively low

quasi-particle poisoning rate but becomes noticeable at a magnitude proximate to the Rabi frequency. As the noise intensity rises, the weight of the secondary peak increases. The primary and secondary peaks merge into a single peak with an increase in noise intensity. This phenomenon is attributed to the quasi-particle poisoning event's alteration of the Majorana parity and the effective tunneling amplitude, resulting in the emergence and amplification of the secondary peak. The double-peak configuration of the power spectrum with a noise intensity of $\Gamma/\Omega = 0.5$ is visually demonstrated in Fig. 4(c).

Subsequently, we present a discussion on inhomogeneous quasi-particle noise. Firstly, we consider the special cases where $\Gamma_1 \neq 0$ and $\Gamma_2 = 0$, as well as $\Gamma_1 = 0$ and $\Gamma_2 \neq 0$. These cases correspond to the scenario where only one Majorana zero mode undergoes a quasi-particle poisoning event. For $\lambda = 1$, the power spectrum is indistinguishable between $\Gamma_1 \neq 0$, $\Gamma_2 = 0$ and $\Gamma_1 = 0$, $\Gamma_2 \neq 0$. By comparing Figs. 5 and 3, the most conspicuous dissimilarity between inhomogeneous quasi-particle noise and homogeneous quasi-particle noise is that for noise intensities much greater than the Rabi oscillation frequency; the fused frequency tends to zero in the former, whereas it tends to $|t_1|$ (also equal to $|t_2|$) in the latter.

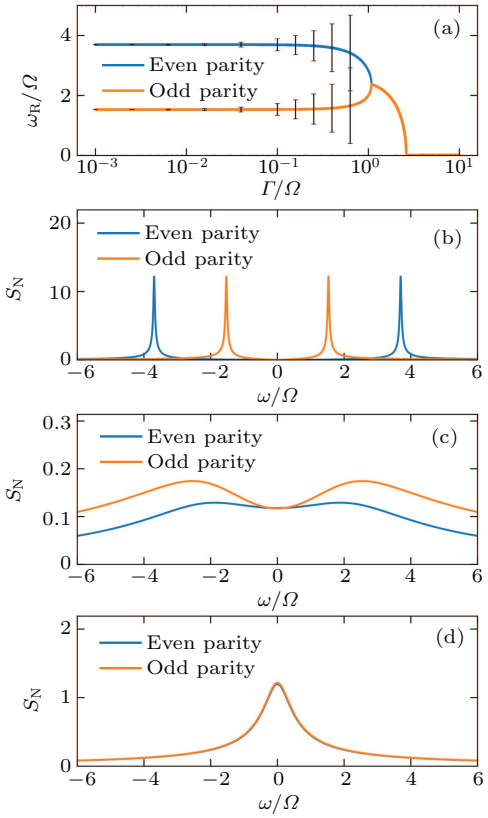


Fig. 3. (a) Peak frequency curve of different parity under quasi-particle noise intensities (Γ/Ω) ranging from 10^{-3} to 10^1, with $\lambda = 1$, $\theta = \pi/4$, $\kappa = 0.002|t_1|$, and $|t_1| = \Omega$. The corresponding Rabi oscillation frequency, denoted as ω_R, is associated with the peak. The error bar in the figures represents the peak width and the main peak of each parity state is shown. The values of κ and θ are held constant throughout the remaining images. (b) Power spectrum for $\Gamma/\Omega = 0.01$. (c) Power spectrum for $\Gamma/\Omega = 1.6$. (d) Power spectrum for $\Gamma/\Omega = 10$.

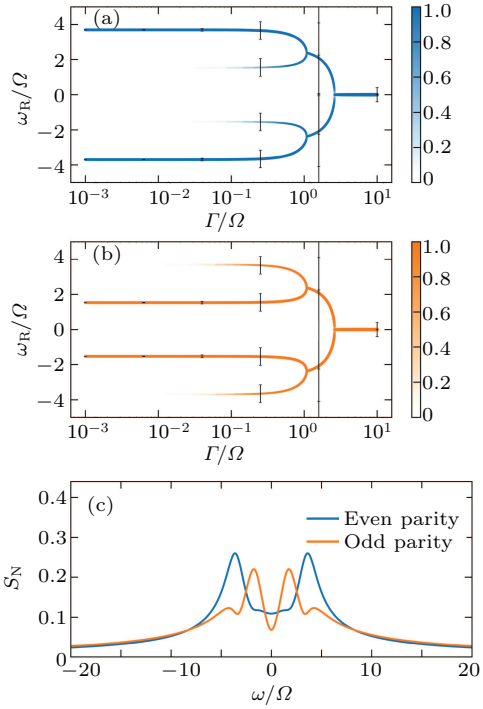


Fig. 4. (a) Peak frequency curve for even parity under quasi-particle noise intensity ranging from 10^{-3} to 10^1, where the color bar presents the relative weight of the peaks. (b) Peak frequency for odd parity under quasi-particle noise intensity ranging from 10^{-3} to 10^1. (c) Power spectrum for $\Gamma/\Omega = 0.5$.

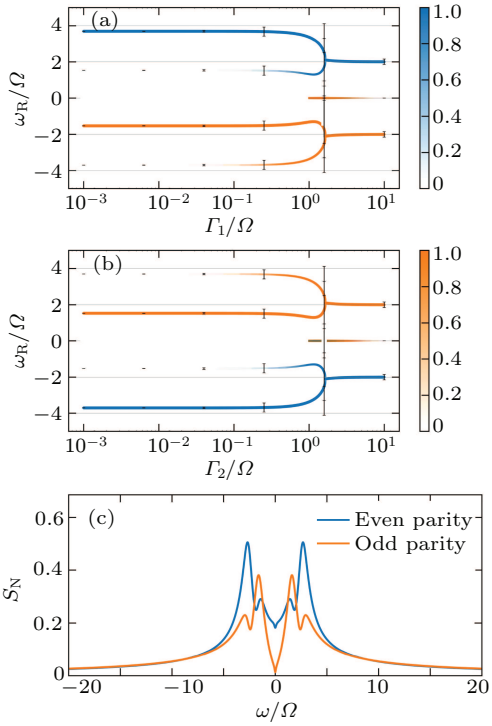


Fig. 5. (a) Peak frequency curve under the influence of quasi-particle noise with intensity represented by Γ_1/Ω, which varies from 10^{-3} to 10^1. Additionally, $\Gamma_2/\Omega = 0$ and the value of λ is set to 1. The frequency diagram exhibits symmetry across the $\omega_R = 0$ axis. Therefore, in (a), to provide a clearer demonstration, we only display even parity for $\omega_R > 0$ and only odd parity for $\omega_R < 0$. Otherwise, the even and odd parity would overlap, decreasing the picture's clarity. (b) Peak frequency curve under the influence of quasi-particle noise with intensity represented by Γ_2/Ω, which varies from 10^{-3} to 10^1, while $\Gamma_1 = 0$ and $\lambda = 1$. Similar to (a), only odd parity is presented for $\omega_R > 0$ and only even parity for $\omega_R < 0$ to enhance clarity. Due to the symmetry of the frequency diagram by the axis $\omega_R = 0$, (a) and (b) are identical. (c) Power spectrum for $\Gamma_1/\Omega = 0.5$.

By comparing Figs. 5 and 3, we observe the difference between inhomogeneous quasi-particle noise and homogeneous quasi-particle noise, but we are unable to differentiate between a single quasi-particle $\hat{\gamma}_1$ ($\Gamma_1 \neq 0$, $\Gamma_2 = 0$), and a single quasi-particle, $\hat{\gamma}_2$ ($\Gamma_2 \neq 0, \Gamma_1 = 0$). This lack of distinction is expected because at $\lambda = 1$, the Majorana modes $\hat{\gamma}_1$ and $\hat{\gamma}_2$ possess full symmetry and thus it is not possible to distinguish between them. If we desire to distinguish between $\hat{\gamma}_1$ and $\hat{\gamma}_2$ in real space, we can set $|t_1| \neq |t_2|$ and break the symmetry between the noise effects of Γ_1 and Γ_2. For instance, when $\lambda = 0.5$, that is $|t_1| = 2|t_2|$, we can define $\hat{\gamma}_1$ and $\hat{\gamma}_2$ in real space, resulting in different spectra for the two types of noise. Additionally, in the high noise region (i.e., $\geq 10^1$), single quasi-particle noise exhibits distinct behavior from homogeneous quasi-particle noise: the Rabi-oscillation frequency no longer tends to zero but converges to $2|t_1|$ for $\Gamma_2 = 0$ and to $2|t_2|$ for $\Gamma_1 = 0$.

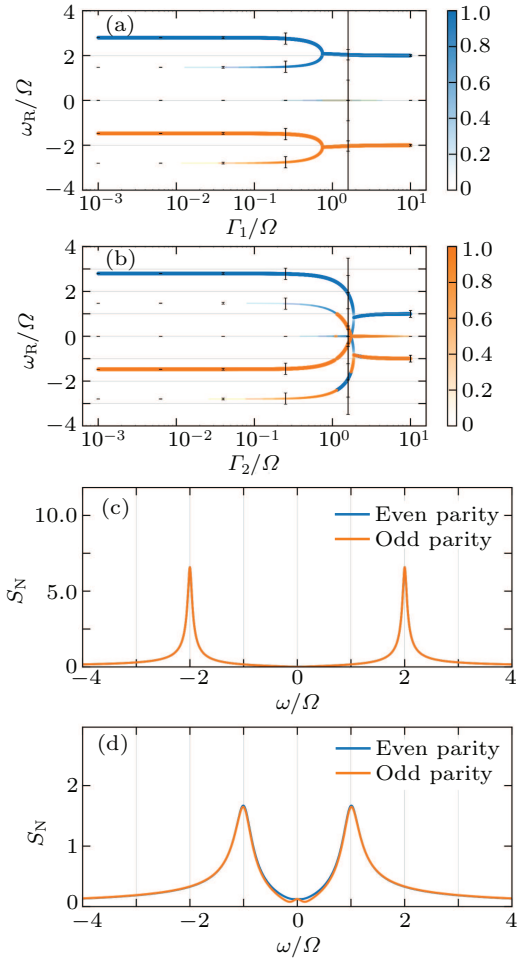


Fig. 6. (a) Peak frequency curve under the influence of quasi-particle noise with intensity represented by Γ_1/Ω, which varies from 10^{-3} to 10^1. Additionally, $\Gamma_2/\Omega = 0$ and the value of λ is set to 0.5. For the sake of enhancing visual clarity, only the width of the peak with a weight greater than 10^{-3} is displayed and only odd parity is displayed for $\omega_R > 0$. Both parities have the same configuration but with different weights, both are symmetry curves along axis $\omega_R = 0$ as displayed in Figs. 4(a) and 4(b), to have a better comparison, only half of each parity is displayed. (b) Peak frequency curve under the influence of quasi-particle noise with intensity represented by Γ_2/Ω, which varies from 10^{-3} to 10^1. Additionally, $\Gamma_1/\Omega = 0$ and the value of λ is set to 0.5. (c) Power spectrum for $\Gamma_1/\Omega = 10$ Here the curve of even parity is almost covered by the curve of odd parity, since they have the same configuration. This situation is the same for (d) and other figures. (d) Power spectrum for $\Gamma_2/\Omega = 10$.

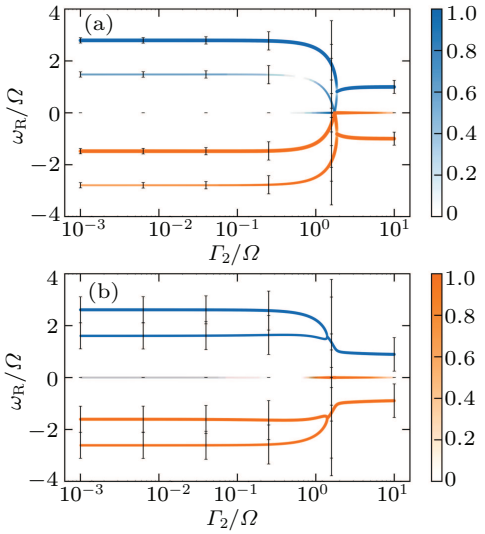


Fig. 7. (a) Peak frequency curve under the influence of quasi-particle noise with intensity represented by Γ_2/Ω, which varies from 10^{-3} to 10^1. Additionally, $\Gamma_1/\Omega = 0.1$ and the value of λ is set to 0.5. (b) Peak frequency curve under the influence of quasi-particle noise with intensity represented by Γ_2/Ω, which varies from 10^{-3} to 10^1. Additionally, $\Gamma_1/\Omega = 0.5$ and the value of λ is set to 0.5.

Subsequently, we explore the case where both Γ_1 and Γ_2 are non-zero and not equal. Specifically, we consider the range of Γ_1/Ω to be between 10^{-3} and 10^1, while Γ_2 remains constant. Moreover, we can set $\Gamma_1 = x + C_1$ with $x \in [10^{-3}, 10^1]$ and $\Gamma_2 = C_2$, or conversely, $\Gamma_2 = x + C_2$ with $x \in [10^{-3}, 10^1]$ and $\Gamma_1 = C_1$, following the approach proposed in Ref. [52]. This yields the possibility of discerning the prevailing quasi-particle noise situation (represented by C_1 and C_2) in the Majorana qubit by observing different behaviors of the power spectrum concerning the variable x. As such, we present a method for detecting noise in the Majorana qubit, with the numerical results serving as a reliable reference for experimental investigations. We demonstrate the peak frequency diagram as an illustrative example in Figs. 7(a) and 7(b). Notably, distinct quasi-particle poisoning leads to different behaviors of ω_R. Specifically, the peak width for $\Gamma_1/\Omega = 0.1$ is considerably narrower than that of $\Gamma_1/\Omega = 0.5$ at the same Γ_2 value. Both peak widths increase with Γ_2 before the fusion point, corresponding to the rising dissipation effect proportional to the total noise rate ($\Gamma_1 + \Gamma_2$). Additionally, we observe that the fusion points for different noise intensities also differ. We denote the fusion point as $F = (\Gamma_F, \omega_{RF})$, with the value of Γ_F for $\Gamma_1/\Omega = 0.5$ being larger than that for $\Gamma_1/\Omega = 0.1$, and the value of ω_{RF} for $\Gamma_1/\Omega = 0.5$ being greater than the value for $\Gamma_1/\Omega = 0.1$. Furthermore, for $\Gamma_1/\Omega = 0.1$, the frequency curves approach zero before fusing, whereas for $\Gamma_1/\Omega = 0.5$, the frequency curve fuses directly, indicating different fusion points. The weight of the secondary peak for

$\Gamma_1/\Omega = 0.5$ is also greater than the weight of the secondary peak for $\Gamma_1/\Omega = 0.1$. Overall, the fusion point, peak width and peak weight serve as reliable indicators for distinguishing different noise types and intensities. Therefore, the theoretical results presented in this study can aid in detecting noise in the Majorana qubit.

4.2. Overlapping with fluctuation

This section explores the effects of overlapping and fluctuations on the power spectrum of the Majorana readout. Firstly, we analyze the impact of pure Majorana overlapping. The Hamiltonian governing the coupling between a Majorana mode and a quantum dot under the particle number basis, with pure Majorana overlapping, can be expressed as

$$\hat{H} = \begin{bmatrix} \varepsilon_{\rm hyb} & t_1^* + \mathrm{i}t_2^* & 0 & 0 \\ t_1 - \mathrm{i}t_2 & -\varepsilon_{\rm hyb} & 0 & 0 \\ 0 & 0 & -\varepsilon_{\rm hyb} & t_1^* - \mathrm{i}t_2^* \\ 0 & 0 & t_1 + \mathrm{i}t_2 & \varepsilon_{\rm hyb} \end{bmatrix}. \tag{33}$$

Based on the Hamiltonian derived earlier, it is evident that pure Majorana overlapping introduces a $2\varepsilon_{\rm hyb}$ energy level space, as expected. The even parity and odd parity of the Majorana are denoted as $|0\rangle_t$ and $|1\rangle_t$, respectively. In an infinitely long nanowire, ideal zero energy degeneracy can be achieved, where the energy level for $|0\rangle_t$ and $|1\rangle_t$ is zero. However, Majorana overlapping leads to a splitting of the degenerate energy level, where the energy level for $|0\rangle_t$ is $-\varepsilon_{\rm hyb}$, and for $|1\rangle_t$ is $\varepsilon_{\rm hyb}$. Denoting $|0\rangle$ and $|1\rangle$ as the dot occupation number of the quantum dot, we use $|01\rangle$ to represent $|0\rangle \otimes |1\rangle_t$. The energy level for $|01\rangle$ is $\varepsilon_{\rm hyb}$, for $|10\rangle$ it is $-\varepsilon_{\rm hyb}$, for $|00\rangle$ it is also $-\varepsilon_{\rm hyb}$ and for $|11\rangle$ it is $\varepsilon_{\rm hyb}$. Therefore, the diagonal elements of the matrix can be obtained. The effective Rabi oscillation frequency can be calculated as $\omega_{\rm R} = 2\sqrt{|t_p|^2 + \varepsilon_{\rm hyb}^2}$. It is observed that for $\varepsilon_{\rm hyb} < 10^{-1}$, pure Majorana overlapping has a negligible influence. For $\varepsilon_{\rm hyb} \geq 1$, the peak frequency increases almost linearly with $\varepsilon_{\rm hyb}$ and the distance between the two parities decreases, while the peak width remains almost unchanged. This indicates that pure Majorana overlapping causes minimal dissipation, which is in accordance with expectations, as illustrated in Fig. 8(a). The influence of $\varepsilon_{\rm hyb}$ on the power spectrum can be observed from Fig. 8. As $\varepsilon_{\rm hyb}$ increases, the weight of the Rabi oscillation peak decreases while the weight of the zero-frequency peak increases. This indicates that Majorana overlapping leads to the shot noise effect. It should be noted that the main difference between pure Majorana overlapping and Majorana overlapping with fluctuation is the width of the peak, which is caused by fluctuation.

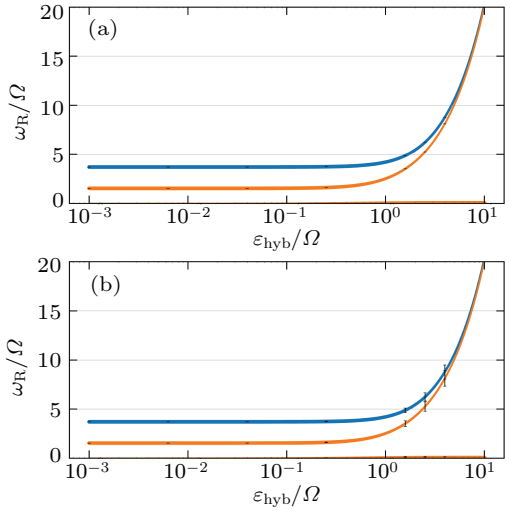


Fig. 8. (a) Peak frequency curve for the scenario of pure Majorana overlapping. It is notable that the diagram possesses a symmetry with respect to $\omega_{\rm R} = 0$; therefore, solely the portion corresponding to $\omega_{\rm R} \geq 0$ is depicted. (b) Peak frequency curve for Majorana overlapping with fluctuation $g^2 = 0.1\varepsilon_{\rm hyb}$.

In Subsection 4.2, the frequency behavior of overlapping and quasi-particle poisoning noise is discussed by varying the quasi-particle injection rate. The proposed approach suggests that the noise in the Majorana qubit can be uniquely identified and labeled by a quaternion array consisting of $(\Gamma_1, \Gamma_2, \varepsilon_{\rm hyb}, g^2)$, which we refer to as the characteristic array for noise. By analyzing the peak width, fusion point, frequency under the quasi-particle poisoning rate limit and curve structure of the frequency curve, we can describe the behavior of the frequency curve. The establishment of a map between the characteristic array for noise and the frequency curve enables theoretical simulations to provide valuable guidance for the detection and characterization of noise in Majorana qubits. In Fig. 9, a comparison is made between different noise parameters. It is observed that, with $\varepsilon_{\rm hyb}/\Omega = 1$, the frequency under a low quasi-particle poisoning rate is higher than the case without Majorana overlapping. Additionally, differences in peak width and weight are visible for Majorana overlapping noise with and without quasi-particle poisoning ($\Gamma_2/\Omega = 0.5$) under a low quasi-particle poisoning rate ($\Gamma_1/\Omega \ll 1$). For $\Gamma_1/\Omega \approx 1$, it is found that, before fusion, the primary peak frequency decreases but does not reach zero for $\varepsilon_{\rm hyb}/\Omega = 1, g^2 = 0.1\varepsilon_{\rm hyb}$, whereas it does reach zero for $\varepsilon_{\rm hyb}/\Omega = 1, g^2 = 0.1\varepsilon_{\rm hyb}, \Gamma_2/\Omega = 0.5$. After fusion, the primary and secondary peaks are in the fused state for $\varepsilon_{\rm hyb}/\Omega = 1, g^2 = 0.1\varepsilon_{\rm hyb}$, but for $\varepsilon_{\rm hyb}/\Omega = 1, g^2 = 0.1\varepsilon_{\rm hyb}, \Gamma_2/\Omega = 0.5$, there is a non-vanishing space between the primary and secondary peaks. While the physical mechanisms underlying these complex curve behaviors are still not fully understood, the differences between the curves offer a promising approach to identifying and characterizing noise in Majorana qubits.

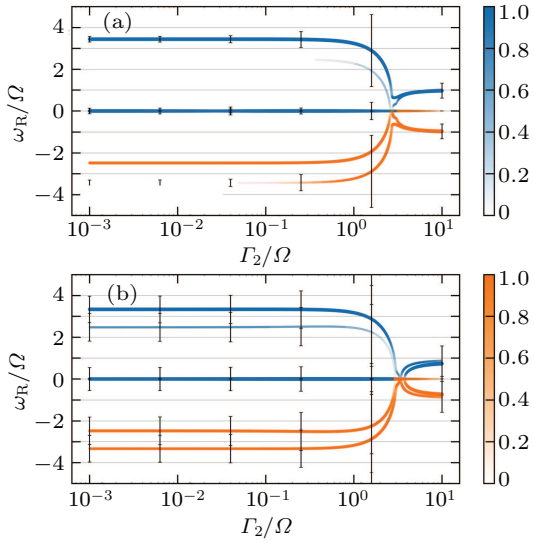


Fig. 9. (a) Peak frequency curve for $\varepsilon_{\rm hyb}/\Omega = 1$, $g^2 = 0.1\varepsilon_{\rm hyb}$ and $\lambda = 0.5$. (b) Peak frequency curve for $\Gamma_2/\Omega = 0.5$, $\varepsilon_{\rm hyb}/\Omega = 1$, $g^2 = 0.1\varepsilon_{\rm hyb}$ and $\lambda/\Omega = 0.5$.

5. Summary and outlook

In this paper, we present a comprehensive analysis of noise in Majorana qubits, wherein we construct a Majorana noise model that incorporates quasi-particle poisoning and Majorana overlapping with fluctuation. Subsequently, we develop a method for continuous Majorana parity measurement, which relies on the quantum jump model. Furthermore, we examine the impact of noise on the readout signal and propose a new approach for detecting the noise situation in Majorana qubits. Our future work aims to expand upon our current findings and refine the mapping between noise parameters and signal curve characteristics, thereby enhancing the rigor of the Majorana noise detection method.

Acknowledgements

We would like to express our gratitude for the valuable discussions with Li Chen, Feng-Feng Song, Gu Zhang and Zhenhua Zhu. This work was supported by the Innovation Program for Quantum Science and Technology (Grant No. 2021ZD0302400), the National Natural Science Foundation of China (Grants No. 11974198), and the Natural Science Foundation of Shandong Province of China (Grant No. ZR2021MA091).

References

[1] Kitaev A 2003 *Annals of Physics* **303** 2
[2] Nayak C, Simon S H, Stern A, Freedman M and Das Sarma S 2008 *Rev. Mod. Phys.* **80** 1083
[3] Fradkin E, Nayak C, Tsvelik A and Wilczek F 1998 *Nuclear Physics B* **516** 704
[4] Stern A and Halperin B I 2006 *Phys. Rev. Lett.* **96** 016802
[5] Bonderson P, Kitaev A and Shtengel K 2006 *Phys. Rev. Lett.* **96** 016803
[6] Nayak C, Simon S H, Stern A, Freedman M and Das Sarma S 2008 *Rev. Mod. Phys.* **80** 1083
[7] Bishara W, Bonderson P, Nayak C, Shtengel K and Slingerland J K 2009 *Phys. Rev. B* **80** 155303
[8] Das Sarma S, Nayak C and Tewari S 2006 *Phys. Rev. B* **73** 220502
[9] Kitaev A Y 2001 *Physics-Uspekhi* **44** 131
[10] Lutchyn R M, Bakkers E P A M, Kouwenhoven L P, Krogstrup P, Marcus C M and Oreg Y 2018 *Nat. Rev. Mater.* **3** 52
[11] Oreg Y, Refael G and von Oppen F 2010 *Phys. Rev. Lett.* **105** 177002
[12] Mourik V, Zuo K, Frolov S M, Plissard S R, Bakkers E P A M and Kouwenhoven L P 2012 *Science* **336** 1003
[13] Rokhinson L P, Liu X and Furdyna J K 2012 *Nat. Phys* **8** 795
[14] Deng M T, Yu C L, Huang G Y, Larsson M, Caroff P and Xu H Q 2012 *Nano Lett.* **12** 6414
[15] Das A, Ronen Y, Most Y, Oreg Y, Heiblum M and Shtrikman H 2012 *Nat. Phys.* **8** 887
[16] Finck A D K, Van Harlingen D J, Mohseni P K, Jung K and Li X 2013 *Phys. Rev. Lett.* **110** 126406
[17] Churchill H O H, Fatemi V, Grove-Rasmussen K, Deng M T, Caroff P, Xu H Q and Marcus C M 2013 *Phys. Rev. B* **87** 241401
[18] Albrecht S M, Higginbotham A P, Madsen M, Kuemmeth F, Jespersen T S, Nygard J, Krogstrup P and Marcus C M 2016 *Nature* **531** 206
[19] Deng M T, Vaitiekenas S, Hansen E B, Danon J, Leijnse M, Flensberg K, Nygard J, Krogstrup P and Marcus C M 2016 *Science* **354** 1557
[20] Lutchyn R M, Sau J D and Das Sarma S 2010 *Phys. Rev. Lett.* **105** 077001
[21] Sau J D, Lutchyn R M, Tewari S and Das Sarma S 2010 *Phys. Rev. Lett.* **104** 040502
[22] Read N and Green D 2000 *Phys. Rev. B* **61** 10267
[23] Alicea J 2012 *Rep. Prog. Phys.* **75** 076501
[24] Leijnse M and Flensberg K 2012 *Semicond. Sci. Technol.* **27** 124003
[25] Aasen D, Hell M, Mishmash R V, Higginbotham A, Danon J, Leijnse M, Jespersen T S, Folk J A, Marcus C M, Flensburg K and Alicea J 2016 *Phys. Rev. X* **6** 031016
[26] Munk M I K, Schulenborg J, Egger R and Flensberg K 2020 *Phys. Rev. Research* **2** 033254
[27] Hassler F, Akhmerov A R, Hou C Y and Beenakker C W J 2010 *New J. Phys.* **12** 125002
[28] Plugge S, Rasmussen A, Egger R and Flensberg K 2017 *New J. Phys.* **19** 012001
[29] Karzig T, Knapp C, Lutchyn R M, Bonderson P, Hastings M B, Nayak C, Alicea J, Flensberg K, Plugge S, Oreg Y, Marcus C M and Freedman M H 2017 *Phys. Rev. B* **95** 235305
[30] Fu L 2010 *Phys. Rev. Lett.* **104** 056402
[31] van Heck B, Lutchyn R M and Glazman L I 2016 *Phys. Rev. B* **93** 235431
[32] Krogstrup P, Ziino N L B, Chang W, Albrecht S M, Madsen M H, Johnson E, Nygard J, Marcus C M and Jespersen T S 2015 *Nat. Mater.* **14** 400
[33] Shabani J, Kjaergaard M, Suominen H J, Kim Y, Nichele F, Pakrouski K, Stankevic T, Lutchyn R M, Krogstrup P, Feidenhans'l R, Kraemer S, Nayak C, Troyer M, Marcus C M and Palmstr C J 2016 *Phys. Rev. B* **93** 155402
[34] Gul O, Zhang H, Bommer J D S, de Moor M W A, Car D, Plissard S R, Bakkers E P A M, Geresdi A, Watanabe K, Taniguchi T and Kouwenhoven L P 2018 *Nat. Nanotech.* **13** 192
[35] Beenakker C 2013 *Annu. Rev. Condens. Matter Phys.* **4** 113
[36] Stanescu T D, Lutchyn R M and Das Sarma S 2011 *Phys. Rev. B* **84** 144522
[37] Sarma S D, Freedman M and Nayak C 2015 *npj Quantum Inf.* **1** 15001
[38] Jiang L, Kane C L and Preskill J 2011 *Phys. Rev. Lett.* **106** 130504
[39] Bonderson P and Lutchyn R M 2011 *Phys. Rev. Lett.* **106** 130505
[40] Hyart T, van Heck B, Fulga I C, Burrello M, Akhmerov A R and Beenakker C W J 2013 *Phys. Rev. B* **88** 035121
[41] Clarke D J, Sau J D and Das Sarma S 2016 *Phys. Rev. X* **6** 021005
[42] Alicea J, Oreg Y, Refael G, von Oppen F and Fisher M P A 2011 *Nat. Phys.* **7** 412
[43] Steiner J F and von Oppen F 2020 *Phys. Rev. Research* **2** 033255
[44] Cao Z, Chen S, Zhang G and Liu D E 2023 *Science China Physics, Mechanics & Astronomy* **66** 267003
[45] Wiseman H M, Utami D W, Sun H B, Milburn G J, Kane B E, Dzurak A and Clark R G 2001 *Phys. Rev. B* **63** 235308
[46] Budich J C, Walter S and Trauzettel B 2012 *Phys. Rev. B* **85** 121405
[47] Karzig T, Cole W S and Pikulin D I 2021 *Phys. Rev. Lett.* **126** 057702
[48] Flensberg K 2011 *Phys. Rev. Lett.* **106** 090503

[49] Cheng M, Lutchyn R M, Galitski V and Das Sarma S 2009 *Phys. Rev. Lett.* **103** 107001
[50] Goldstein G and Chamon C 2011 *Phys. Rev. B* **84** 205109
[51] Rainis D and Loss D 2012 *Phys. Rev. B* **85** 174533
[52] Wang C, Gao Y Y, Pop I M, Vool U, Axline C, Brecht T, Heeres R W, Frunzio L, Devoret M H, Catelani G, Glazman L I and Schoelkopf R J 2014 *Nat. Commun.* **5** 5836
[53] Knapp C, Beverland M, Pikulin D I and Karzig T 2018 *Quantum* **2** 88
[54] Knapp C, Karzig T, Lutchyn R M and Nayak C 2018 *Phys. Rev. B* **97** 125404
[55] Ralph T C *Howard Wiseman and Gerard Milburn: Quantum measurement and control* [J]. Springer US, 2012(1)
[56] Marlan O Scully and Zubairy M S 1997 *Quantum Optics* (Cambridge: Cambridge University Press)
[57] Khindanov A, Pikulin D and Karzig T 2021 *SciPost Phys.* **10** 127
[58] Plenio M B and Knight P L 1998 *Rev. Mod. Phys.* **70** 101
[59] Wiseman H M and Milburn G J 1993 *Phys. Rev. A* **47** 1652
[60] Wiseman H M and Milburn G J 1993 *Phys. Rev. Lett.* **70** 548
[61] Goan H S, Milburn G J, Wiseman H M and Bi Sun H 2001 *Phys. Rev. B* **63** 125326
[62] Chang A M, Baranger H U, Pfeiffer L N, West K W and Chang T Y 1996 *Phys. Rev. Lett.* **76** 1695
[63] Goan H S and Milburn G J 2001 *Phys. Rev. B* **64** 235307
[64] Gurvitz S A 1997 *Phys. Rev. B* **56** 15215